

Epsilon near zero based phenomena in metamaterialsAlexey A. Basharin,^{1,2,*} Charalampos Mavidis,^{1,3} Maria Kafesaki,^{1,3} Eleftherios N. Economou,^{1,4} and Costas M. Soukoulis^{1,5}¹*Institute of Electronic Structure and Laser (IESL), Foundation for Research and Technology Hellas (FORTH), P.O. Box 1385, 71110 Heraklion, Crete, Greece*²*National Research University "Moscow Power Engineering Institute," 112250 Moscow, Russia*³*Department of Materials Science and Technology, University of Crete, 71003 Heraklion, Greece*⁴*Department of Physics, University of Crete, 71003 Heraklion, Greece*⁵*Ames Laboratory-USDOE, and Department of Physics and Astronomy, Iowa State University, Ames, Iowa 50011, USA*

(Received 30 October 2012; revised manuscript received 7 March 2013; published 16 April 2013)

We present and analyze unique phenomena of enhanced transmission through systems of subwavelength dielectric cylinders embedded in an epsilon near zero host. Our analysis shows that these phenomena are due to Mie-resonance modes arisen in the dielectric cylinders. Subwavelength waveguides and lenses are proposed based on coupling of these modes between neighboring cylinders. Finally, the proposed phenomena and their possible applications are numerically demonstrated in the THz regime in a realistic polaritonic material of LiF rods in KCl.

DOI: [10.1103/PhysRevB.87.155130](https://doi.org/10.1103/PhysRevB.87.155130)

PACS number(s): 78.67.Pt, 42.25.Bs

I. INTRODUCTION

The area of metamaterials emerged from a paper by Veselago¹ and attracted renewed interest due to the works by Pendry.² Metamaterials are characterized by unusual phenomena and properties, not encountered in natural materials. In particular, there are metamaterials with both negative electrical permittivity and magnetic permeability, and thus negative refractive index,¹⁻⁸ there are also giant permittivity metamaterials⁹ or giant permeability, etc.

A category of metamaterials which has attracted increased attention recently is metamaterials with permittivity near zero (ENZ), or both permittivity and permeability near zero, i.e., zero index metamaterials (ZIM). The increased attention to those materials is due to their intriguing properties.¹⁰⁻²⁵ Namely, ultranarrow ENZ channels can "squeeze" electromagnetic (EM) waves at will.¹⁰⁻¹⁴ Such an effect was also demonstrated experimentally.^{13,14} Total transmission without changing the phase, forming a plane wave front, by using matched impedance zero-index metamaterials, was also shown theoretically.¹⁵

It is worth mentioning that to achieve small negative permittivity values or permittivity near zero, one is not essential to resort to metamaterials. Materials with small negative and near zero permittivity in the THz regime are already available in nature. Such materials are polaritonic materials.^{26,27} These are ionic crystals where an incident electromagnetic (EM) wave excites and couples with optical phonons supported by the crystal.²⁶ As a result, the permittivity of such materials obeys a Lorenz dispersion model;²⁷ at frequencies below their plasma frequency (in the THz regime; frequency at which one of the ionic sublattices moves longitudinally against the other) these materials exhibit negative values of the real part of the permittivity, a feature which may be exploited in achieving plasmonic phenomena or metamaterial properties in structures of simple geometries (note that the permittivity of metals in the THz has very large negative values, making essential the fabrication of complicated-shape inductive elements as to adjust the structure impedance with that of the free space). Moreover, close to the plasma frequency the real part of the permittivity in polaritonic materials is near

zero, allowing the observation of a variety of interesting phenomena and applications associated with ENZ materials and metamaterials.

Such phenomena are total transmission and total reflection of EM waves through ENZ or ZIM materials with embedded proper defects, as proposed by some researchers. In particular, Hao *et al.*¹⁶ analytically and numerically demonstrated that embedding perfect electric conductor (PEC) defects into a ZIM region yields super-reflection (the incident wave is totally blocked) of EM waves incident in that region. Nguyen *et al.*¹⁷ investigated the case of dielectric cylindrical defects placed into a ZIM. The proposed structure allowed us to achieve total transmission and total reflection effects. Similar phenomena have been observed in an ENZ region with dielectric defects, as established by Xu and Chen¹⁸ for excitation of the structure by a TM-polarized wave. These phenomena were predicted analytically and numerically.

In this paper we show numerically that an ordered linear arrangement of dielectric subwavelength cylindrical scatterers embedded in an ENZ host acts as a narrow subwavelength channel where the wave propagates by being transferred from scatterer to the next scatterer. The net result is a very efficient narrow subwavelength waveguide which is capable of operating even in the presence of corners with a minimum backscattering; this narrow channel also provides the basis of building lenses with subwavelength resolution. Besides our numerical demonstration of such important functioning, we propose real composite materials, such as self-organized polaritonic systems, at which the above mentioned phenomena can be observed. Finally, we reveal the physics underlying this electromagnetic wave propagation along a narrow channel consisting of a linear succession of scatterers (reminiscent of the one-dimensional tight-binding electronic transfer from atom to atom): It is due to the appearance at each scatterer of a very sharp Mie resonance (which in the limit of zero-host permittivity becomes a true eigenstate, analogous to the p_x atomic orbital). This resonance also leads to almost total transmission in systems of dielectric scatterers embedded in ENZ media. We confirm this physical picture in the next section by performing both numerical and analytical

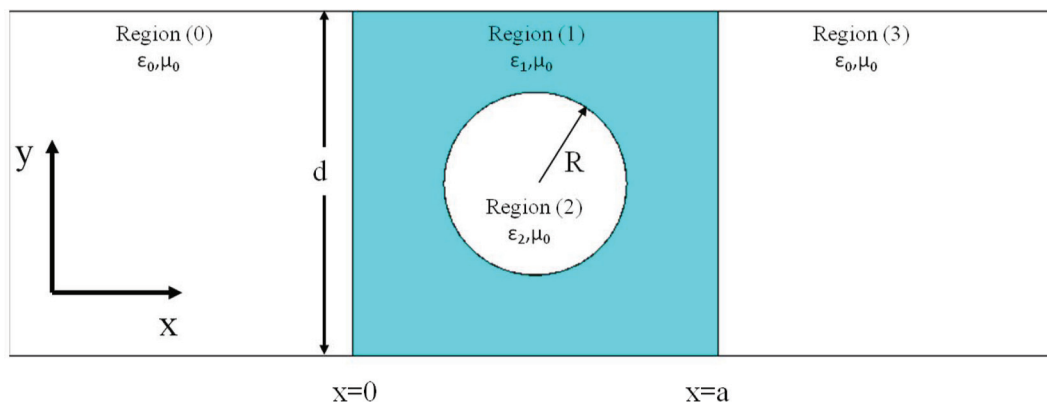


FIG. 1. (Color online) Geometry of the unit cell of our periodic system along the y direction; the unit cell consists of an ENZ region (1) and an embedded dielectric cylinder [region (2)]. The left and right materials surrounding region (1) are considered as air. The upper and bottom boundary conditions of the unit cell are equivalent to a perfect magnetic conductor (PMC) in the case of TE polarization. The geometrical values are typically as follows: $R = 4 \mu\text{m}$, $d = 30 \mu\text{m}$, and $a = 100 \mu\text{m}$.

calculations in a prototype system consisting of a finite slab of ENZ material in which a single cylindrical scatterer is embedded with periodic boundary conditions (BCs) along the y direction (see Fig. 1).

II. TRANSMISSION AND REFLECTION IN ENZ STRUCTURES WITH EMBEDDED DIELECTRIC CYLINDERS—RESONANT TOTAL TRANSMISSION

The structure forming the basis of our investigations here is shown in Fig. 1 and consists of four distinct regions: Regions (0) and (3) are filled with air and are separated by an epsilon near zero (ENZ) ($\epsilon_1 \approx 0$) region (1). A dielectric cylindrical scatterer [region (2)] with radius R is embedded inside region (1) and has permittivity ϵ_2 . We focus on nonmagnetic materials, i.e., the permeability in all regions is the vacuum permeability $\mu = \mu_0$. The upper and bottom walls of the system in our numerical investigations are set to be perfect magnetic conductors in the case of TE polarization; these boundary conditions are in the present case equivalent to a periodic arrangement of cylinders along the y direction with a period d and, hence, they allow us to restrict our study of the propagation of TE electromagnetic waves (either numerically or analytically) only within the strip of width d as shown in Fig. 1.

We consider an EM wave impinging at normal incidence from the left into the unit cell illustrated in Fig. 1. Such a wave will be of the form $\vec{E}_{\text{inc}} = E_0 \hat{z} e^{i(k_0 x - \omega t)}$ for TE polarization. We will omit the time variation $e^{-i\omega t}$ throughout the rest of the paper and we shall set $E_0 = -i\omega\mu$.

A. Case in the absence of cylinder

We examine first the case without the cylinder, i.e., R being set equal to zero. Thus the problem reduces to a plane wave incident on a uniform and isotropic ENZ slab (1) located between two uniform and isotropic regions (0) and (3).

Based on the solution of problem 4, p. 299 of Ref. 28, the fields in region (0) can be written as

$$\vec{E} = -i\omega\mu\hat{z}(e^{ik_0x} + \rho e^{-ik_0x}), \quad (1a)$$

$$\vec{H} = \frac{1}{i\omega\mu} \nabla \times \vec{E} = ik_0\hat{y}(e^{ik_0x} - \rho e^{-ik_0x}), \quad (1b)$$

while the electromagnetic fields in region (3) are of the form

$$\vec{E} = -i\omega\mu\hat{z}t e^{ik_0(x-a)}, \quad (2a)$$

$$\vec{H} = ik_0\hat{y}t e^{ik_0(x-a)}, \quad (2b)$$

with k_0 as the wave vector of free space $k_0 = \omega/c$. In the above relations ρ and t are reflection and transmission amplitudes (in the absence of the cylinder), which can be calculated by matching the parallel components of the fields E_z and H_y at the boundaries of the system $x = 0$ and $x = a$. For region (1) the electric and magnetic fields must satisfy the Maxwell equation $\vec{E} = -(1/i\omega\epsilon_1)\nabla \times \vec{H}$. Taking into account that ϵ_1 tends to zero, we can conclude that $\nabla \times \vec{H}$ must vanish in order to keep the electric field finite.¹⁰ Besides the relation $\nabla \times \vec{H} = 0 \Rightarrow \vec{H} = -\nabla\phi + \vec{a}$ (with ϕ a scalar potential and \vec{a} a constant vector), we must satisfy the relation $\nabla \cdot \vec{H} = 0 \Leftrightarrow \nabla^2\phi = 0$. Thus, the gradient of any potential ϕ satisfying the Laplace equation can be added to $\vec{H} = \vec{a}$ and the equations $\nabla \times \vec{H} = 0$ and $\nabla \cdot \vec{H} = 0$ will still be satisfied. However, in the present case, based on problem 4 of Ref. 28, we conclude that $H_y = \text{const.} = H_1$, and $H_x = 0$ in region (1) in the absence of the cylinder and for $k_1 \rightarrow 0$. Indeed, according to Ref. 28 and for normal incidence, the magnetic field in region (1) in the absence of the cylinder is of the form $(A_1 e^{ik_1x} + A'_1 e^{-ik_1x})\hat{y}$; but $k_1 = \omega n_1/c = 0$ for $n_1 = 0$. Hence, $\vec{H} = (A_1 + A'_1)\hat{y} \equiv H_1\hat{y}$, where $H_1 = A_1 + A'_1$ and A_1, A'_1 are constants. Moreover, electric and magnetic fields in region (1) should satisfy equation $\vec{H} = (1/i\omega\mu)\nabla \times \vec{E}$, which taking into account that $\vec{H} = H_1\hat{y}$ and that $\vec{E} = E_z\hat{z}$ gives $\partial E_z/\partial x = -i\omega\mu H_1$. Integrating this last relation, we obtain the fields in ENZ region (1):

$$\vec{E} = -i\omega\mu\hat{z}(H_1x - E_1), \quad (3a)$$

$$\vec{H} = \hat{y}H_1, \quad (3b)$$

where H_1, E_1 are constant unknown coefficients.

Applying the boundary conditions, i.e., equating the tangential components of the magnetic and electric fields at the interfaces $x = 0$ and $x = a$, gives simple relations for all the

unknown coefficients of the problem:

$$\begin{aligned} t &= \frac{1}{1 - ik_0 \frac{a}{2}}, & H_1 &= ik_0 t, \\ E_1 &= \frac{ik_0 a - 1}{1 - ik_0 \frac{a}{2}}, & \rho &= -\frac{ik_0 a}{2 - ik_0 a}. \end{aligned} \quad (4)$$

B. Case in the presence of cylinder

Let us consider now the dielectric cylinder [region (2)] embedded in region (1), as shown in Fig. 1. The solutions we have obtained up to now in region (1) in the absence of the cylinder can serve as the ‘‘incident’’ wave to be scattered by the cylinder. This scattered field will be scattered next at the plane segments of width d for $x = 0$ and $x = a$. This process will go on back and forth giving rise to a complicated multiple scattering process. We shall include this multiple scattering process assuming that the fields are almost constant at $x = 0$ and $x = a$ for the width d . As we shall show later on, this is a very reasonable approximation if $R \ll (d/2) \ll a/2$.

We shall proceed now with the first order scattering by the cylinder of the incident wave as described by Eqs. (3a), (3b), and (4). The fields in region (2) inside the cylinder obey vector Helmholtz equation $\nabla \times (\nabla \times \vec{E}) = k_2^2 \vec{E}$.²⁹ Due to its cylindrical shape it is convenient to write the solutions of this equation as an infinite sum of Bessel functions times exponential functions of the angle θ :

$$\vec{E} = -i\omega\mu\hat{z} \sum_{m=-\infty}^{\infty} A_m J_m(k_2 r) e^{im\theta}.$$

(Note that the position vector \vec{r} is measured from the center of the cylinder.) Since the incident electric field as given by Eq. (3a) is proportional to $x = (a/2) + r \cos \theta$ plus a constant, we have to keep only the terms with $m = 1$, $m = 0$, and $m = -1$ (with properly related coefficients A_m) to produce the necessary θ dependence. Thus

$$\vec{E} = -i\omega\mu\hat{z} A J_1(k_2 r) \cos \theta - i\omega\mu\hat{z} A_o J_0(k_2 r), \quad (5a)$$

with $A = 2A_1 = -2A_{-1}$ a constant to be determined from the continuity of the electric field and the tangential component of the magnetic field at the boundary of the cylinder. Using the equation $\vec{H} = (1/i\omega\mu)\nabla \times \vec{E}$ and Eq. (5a) we obtain

$$\vec{H} = \frac{1}{r} \hat{r} A J_1(k_2 r) \sin \theta + \hat{\theta} k_2 [A J_1'(k_2 r) \cos \theta + A_o J_0'(k_2 r)] \quad (5b)$$

(the derivatives in the Bessel functions J_1 and J_0 , denoted by a prime, are with respect to their argument).

The ‘‘incident’’ field to the cylinder is to first order equal to the field in region (1) in the absence of the cylinder as given by Eqs. (3a), (3b), and (4). Therefore, the total fields to this order in region (1) satisfying Maxwell equations are obtained by combining the incident field determined by formulas (3) and the scattered field in which we keep only the term proportional to $\cos(\theta)$ plus a term independent of θ . These scattered fields are of the form of Eqs. (5a) and (5b) with the Bessel functions replaced by the Hankel functions $H_n^{(1)}(z)$ as the value of the variable $z = k_1 r$ approaches zero. To simplify the notation we

shall set $H_n^{(1)}(z) \equiv X_n(z)$. Thus

$$\vec{E}_{sc} = -i\omega\mu\hat{z} A_{1s} X_1(z) \cos \theta - i\omega\mu\hat{z} A_{0s} X_0(z), \quad (6a)$$

$$\vec{H}_{sc} = \frac{1}{r} \hat{r} A_{1s} X_1(z) \sin \theta + \hat{\theta} k_1 [A_{1s} X_1'(z) \cos \theta + A_{0s} X_0'(z)], \quad (6b)$$

where A_{1s} and A_{0s} are constants to be determined by the boundary conditions at $r = R$. The lowest order incident fields in cylindrical coordinates $x = (a/2) + r \cos \theta$ and $y = r \sin \theta$ are $\vec{E}_{inc} = i\omega\mu\hat{z} [E_1 - (a/2)H_1 - H_1 r \cos \theta]$ and $\vec{H}_{inc} = H_1 (\hat{r} \sin \theta + \hat{\theta} \cos \theta)$. Thus, to lowest order the total field, ‘‘incident’’ plus scattered, in region (1) are

$$\begin{aligned} E_z &= -i\omega\mu \left(H_1 \frac{a}{2} - E_1 \right) - i\omega\mu H_1 r \cos \theta \\ &\quad - i\omega\mu A_{1s} X_1(z) \cos \theta - i\omega\mu A_{0s} X_0(z), \end{aligned} \quad (7a)$$

$$H_r = H_1 \sin \theta + \frac{1}{r} A_{1s} X_1(z) \sin \theta, \quad (7b)$$

$$H_\theta = H_1 \cos \theta + A_{1s} k_1 X_1'(z) \cos \theta + A_{0s} k_1 X_0'(z).$$

The continuity of E_z and H_θ for $r = R$ leads to the following equations:

$$A_{1s} = 2H_1 R Q / \{X_1(z_1) - z_1 X_1'(z_1) - Q[X_1(z_1) + z_1 X_1'(z_1)]\}, \quad (8a)$$

$$A_{0s} \equiv \eta \bar{A}_{0s} = \eta z_2 J_0'(z_2) / [J_0(z_2) z_1 X_0'(z_1) - X_0(z_1) z_2 J_0'(z_2)], \quad (8b)$$

where

$$\eta \equiv H_1 \frac{a}{2} - E_1 = 1, \quad Q \equiv \frac{H_2}{H_1 R^2} = \frac{J_1(z_2) - z_2 J_1'(z_2)}{J_1(z_2) + z_2 J_1'(z_2)}, \quad (9)$$

$$z_2 = k_2 R, \quad z_1 = k_1 R.$$

The differentiation denoted by the prime is with respect to the argument.

The first order scattered wave by the cylinder reaches the plane segments at $x = 0$ and $x = a$, it is reflected back to region (1) [the effects of which (to lowest order) are to add terms as in Eqs. (3a) and (3b) with H_1 and E_1 replaced by H_1' and E_1'] and it is transmitted to the regions $x < 0$ and $x > a$. These transmitted waves, as a result of Snell’s law, propagate along the $\mp x$ direction in the limit $k_1 \rightarrow 0$, and for $x = 0^-$ and $x = a^+$, respectively; their amplitudes depend on y or equivalently on the angle θ . However, this dependence is very weak around $y = 0$ (or equivalently, around the $\theta = \pi$ and $\theta = 0$), varying as $\delta \theta^4$, where $\delta \theta = \theta - \pi$ or θ , respectively. Thus, for a range of values of $|y|$ less than $d/2$, the amplitude of the transmitted to the vacuum waves is almost constant, i.e., to a very good approximation and for $|y| \leq d/2$ they behave as plane waves propagating along the $\pm x$ direction. As was pointed out before, these transmitted waves for $0 \leq |y| \leq d/2$ are associated with additional waves reflected back to region (1) approximately of the form of Eqs. (3a) and (3b). These additional reflected [to region (1)] and transmitted (to the vacuum) waves will be approximated by their values at $y = 0$ (i.e. at $\theta = \pi$ and at $\theta = 0$) and for $x = 0$ and $x = a$. These additional reflected to region (1) fields of the form $\vec{E} = -i\omega\mu\hat{z} (H_1^{(1)} x - E_1^{(1)})$, $\vec{H} = \hat{y} H_1^{(1)}$ will create additional second order scattered by the cylinder waves which in turn will

be reflected back to region (1) giving rise to second order terms approximately of the form $\vec{E} = -i\omega\mu\hat{z}(H_1^{(2)}x - E_1^{(2)})$ and $\vec{H} = \hat{y}H_1^{(2)}$ and so on. Summing the resulting geometric series, we obtain the total field (to all orders) within region (1). This total field will modify the reflection ρ and the transmission t in the absence of the cylinder to the following values of $\bar{\rho}$ and \bar{t} , respectively:

$$\bar{t} = \frac{1}{1-iw} + \frac{\Gamma_1}{1-iw}[X_1(s) - sX_1'(s)] + \frac{\Gamma_0}{iw}sX_0'(s), \quad (10a)$$

$$\bar{\rho} = \frac{-iw}{1-iw} - \frac{\Gamma_1}{1-iw}[X_1(s) - sX_1'(s)] + \frac{\Gamma_0}{iw}sX_0'(s), \quad (10b)$$

where $s = k_1a/2$, $w = k_0a/2$, and

$$\Gamma_1 = A_{1s}/(1-M), \quad (10c)$$

$$\Gamma_0 = A_{0s}/(1+K), \quad (10d)$$

$$M = A_{1s}[X_1(s) - sX_1'(s)/iw], \quad (10e)$$

$$K = A_{0s}[X_0(s) - sX_0'(s)/iw]. \quad (10f)$$

Notice that besides omitting the y dependence for $0 \leq |y| \leq d/2$ and keeping the s and z_1 small but finite ($s \approx 0.02$ and $z_1 \approx 0.002$), in Eqs. (3) we have taken the limit $k_1 \rightarrow 0$, we have implicitly used another approximation as well. Indeed, up to now we have taken into account (approximately) the propagation and multiple scattering along the x direction (i.e., for θ around 0 and π) and we have ignored the propagation around $\theta = \pm\pi/2$. This omission is reasonable for the terms associated with J_1 and X_1 since these terms are proportional to $\cos(\theta)$, as shown in Eqs. (6a) to (8b) and $\cos(\theta) \approx 0$ for $\theta \approx \pm\pi/2$. But the θ -independent terms proportional to J_0 and X_0 in Eqs. (6a) to (8b) are not negligible in the directions $\theta \approx \pm\pi/2$; hence, a propagation along the $\theta \approx \pm\pi/2$ direction takes place which also has to be taken into account in view of the periodicity in the y direction; this periodicity implies that there will be incident waves to the cylinder located at the $n = 0$ unit cell coming from all the other cylinders located at the unit cells of $n \neq 0$ since all these other cylinders will emit scattered radiation along the y direction due mainly to their θ -independent part. These additional incident waves on the $n = 0$ cylinder will produce additional scattering along the x direction (due mainly to the θ -independent term) and, hence, will renormalize the coefficient Γ_0 appearing in the transmission and reflection formulas. This renormalization is taken into account only to first order (i.e., by omitting multiple scattering effects involving waves propagating in the y direction) as described in the Appendix.

Analyzing the transmission formula (10a) it results in the conclusion that the transmission coefficient becomes resonant, leading to large $|\bar{t}|$ values, at the poles of the quantity Q of Eq. (9), i.e., where the denominator of Q vanishes. This happens when $J_1(k_2R) = -k_2RJ_1'(k_2R)$, which can be recast to $J_0(k_2R) = 0$ [resulting by applying the recurrence relation $J_1'(k_2R) = J_0(k_2R) - (1/k_2R)J_1(k_2R)$]. It follows that a resonance at the transmission coefficient $|\bar{t}|$ will appear whenever $z = k_2R$ coincides with any of the zeros of the Bessel function $J_0(z)$; the lowest resonance will appear when $k_2R = 2.404826$ or $\lambda_2 = 1.306 D$, $D = 2R$. Another

resonance, but a broader one and at lower frequency, will appear when \bar{A}_{0s} [see Eq. (8b)] exhibits a resonance behavior. This resonance is associated with a cylindrically symmetric scattered wave and its shape and frequency are affected by the coupling of the cylinders along the y direction, as is shown in Fig. 2.

In Fig. 2 we compare our analytic results [Figs. 2(b) and 2(d)] based on Eqs. (8a) to (10f) for the EM transmission amplitude $|\bar{t}|$ in the system shown in Fig. 1 with the corresponding accurate results [Figs. 2(a) and 2(c)] obtained by solving numerically Maxwell's equations with the Microwave Studio (MW) commercial software, for $R = 4 \mu\text{m}$, $\varepsilon_2 = 40\varepsilon_0$, $\varepsilon_1 = 0.001\varepsilon_0$, and $a = 100 \mu\text{m}$. We present both cases of large d (where the couplings along the y direction are negligible) and the small d (where these couplings are appreciable). In the case of large d the analytical results practically coincide with the numerical ones [see Figs. 2(a) and 2(b)] thus justifying the various approximations we employed in deriving Eqs. (8a) to (10f). In the case of small d [Figs. 2(c) and 2(d)], in spite of using the renormalized Γ_0 as a result of the couplings in the y direction, there are appreciable differences which, for the low frequency resonance, we attribute to our omission of the multiple-scattering effects along the $\theta \approx \pm\pi/2$ direction (see the Appendix), while for the resonance at $f = 4.54$ THz, to our complete neglect of the couplings along the $\theta \approx \pm\pi/2$ direction, which in any case are weak as shown by the sharpness of the resonance peak. We plot also in Fig. 2(a) the EM transmission amplitude for the system shown in Fig. 1 in the absence of the cylinder [dashed line in Fig. 2(a)]. We also draw an inset in Fig. 2(a) showing the direction of the electric field at the second resonance at 4.54 THz.

Focusing on Figs. 2(a) or 2(b), one can clearly see two resonances. A broad one at around 1.5 THz, which broadens and moves to lower frequencies, tending to disappear, as one reduces the distance of the cylinders along the y direction [compare Figs. 2(a) to 2(c)], increasing the coupling of those cylinders. This resonance comes from the resonance of the \bar{A}_{0s} of Eq. (8b) and corresponds to a cylindrically symmetric wave. The second resonance at 4.54 THz is the resonance coming from the condition $J_0(k_2R) = 0$ mentioned above, and corresponds to asymmetric field distribution along x , as shown in the inset of Fig. 2(a).

This second resonance is the resonance of interest in the present work and responsible for the impressive waveguide feature presented below. This is because it is this resonance that is very sharp even for rather small d [see Fig. 2(c)], it is strongly confined in the y direction and it couples efficiently with identical resonances appearing in cylinders along the x direction as we shall show later. The nature of this resonance is of Mie type and occurs when the wavelength inside the cylinder is about equal to the average between its diameter and half of its circumference. In the present case, where the electrical permittivity of the scatterer is much higher than the permittivity of the surrounding medium, the resonance becomes very sharp and tends to coincide with the corresponding natural EM mode in the cylindrical scatterer; this mode is associated with strong displacement currents inside the scatterer, leading to the possibility of a high magnetic field. Similar resonances have been described in the paper by O'Brien and Pendry³⁰ for high-index dielectric cylinders when the polarization of

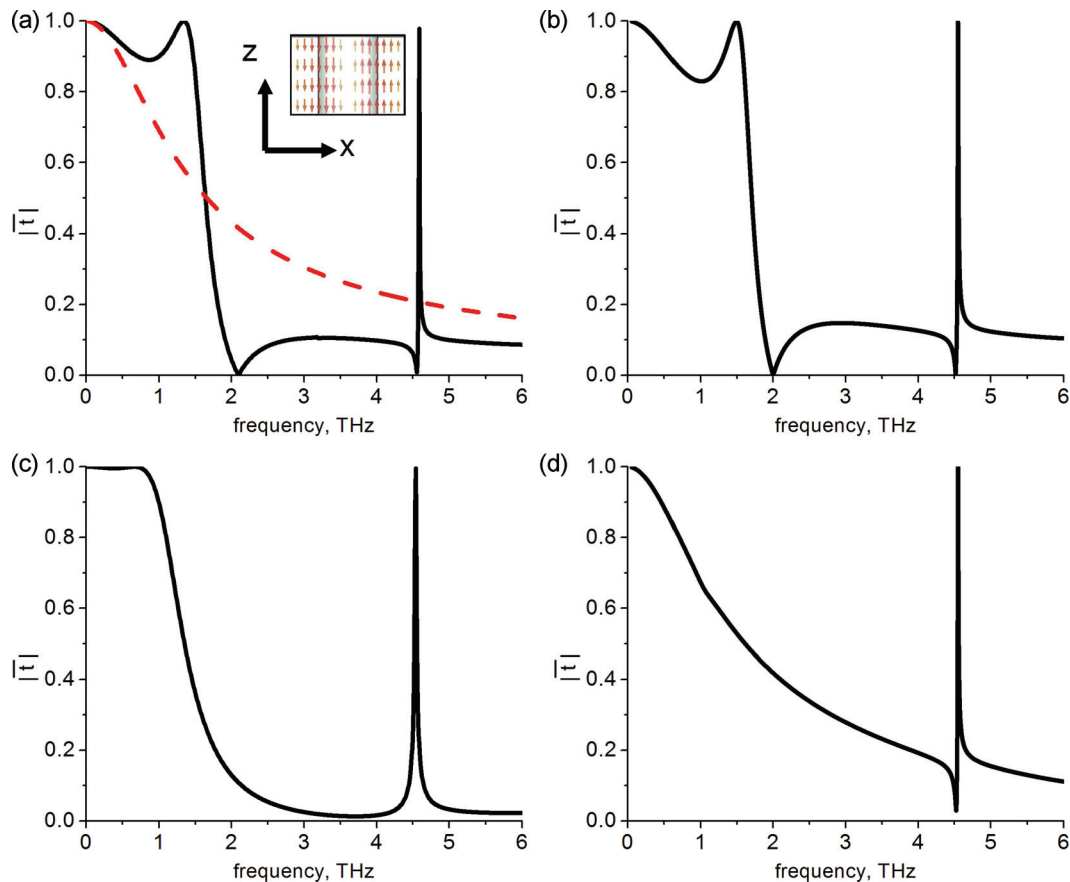


FIG. 2. (Color online) Comparison of the results for the transmission amplitude $|t|$ based on Eqs. (8a) to (10f) with the numerical results based on the Microwave Studio (MWS) for the system of the unit cell which is shown in Fig. 1 with $R = 4 \mu\text{m}$, $\epsilon_1 = 0.001\epsilon_0$, $\epsilon_2 = 40\epsilon_0$, and $a = 100 \mu\text{m}$. (a) Large d , $d = 100 \mu\text{m}$, MWS. (b) Large d , formulas (8a) to (10f). (c) $d = 30 \mu\text{m}$, MWS. (d) $d = 30 \mu\text{m}$, formulas (8a) to (10f) including the renormalization due to couplings along the y direction (see text). The incident wave is a TE polarized wave (i.e., \vec{E} along the axis of the cylinder). Dashed line shows the corresponding transmission for the system with no cylinder. The sharpness of the resonance is due to the large ratio ϵ_2/ϵ_1 and the omission of any losses. The inset shows the displacement currents and the electric field distribution of the sharp resonant mode at the frequency 4.54 THz.

electric field is perpendicular to the axis of the cylinder. In the case of Ref. 30 and for the zeroth-order resonance only, the azimuthally directed displacement current is enhanced which results in an enhanced magnetic field along the cylinder axis. This enhanced magnetic field can lead to artificial magnetism in a composite consisting of such a system of cylinders.³⁰ Moreover, Peng *et al.*³¹ theoretically and experimentally demonstrated the existence of a Mie resonance in the case of the electric field being parallel to the axis of a high-index dielectric cylinder. Also, it is well known from other theoretical and experimental studies of the appearance of Mie resonances in subwavelength particles.³²⁻³⁵

To demonstrate more clearly the potential of the above mentioned resonance (at 4.54 THz) to provide subwavelength guiding, we also show the field distributions at the x - y plane, at the resonance, and in the case of a single cylinder embedded in an ENZ ($\epsilon_1 = 0.001\epsilon_0$) matrix as calculated by Microwave Studio. Figure 3(a) shows the E_z field while Fig. 3(b) shows the magnetic field H_y distribution for TE polarized incident wave. As seen in Fig. 3(a), the electric field E_z is concentrated along the x direction, with two lobes of opposite sign resembling the form of a p_x atomic orbital. This field, for large ϵ_2 , leads to

large displacement currents of opposite direction at the two x sides of the cylinder (see also the inset in Fig 2), which yield a strong magnetic field [see Fig. 3(b)] and lead to a dramatic increase of the transmission at 4.54 THz compared with the case of no cylinder [dashed line in Fig. 2(a)].

III. SUBWAVELENGTH GUIDING AND LENSES WITH SUBWAVELENGTH RESOLUTION BASED ON ENZ PHENOMENA

The p_x -like form of the electric field at the cylinder Mie resonance discussed in the previous section suggests the possibility of subwavelength guiding of an EM wave in a chain of such cylinders along the x direction using the coupling of the waves/modes belonging to neighboring cylinders (in a way similar to electron propagation along a one-dimensional chain of atoms by employing the tight-binding scheme consisting of p_x atomic orbitals). Such a subwavelength guiding is confirmed in Fig. 4(a), in a chain of cylinders of radius $R = 4 \mu\text{m}$ and permittivity $\epsilon_2 = 40\epsilon_0$ embedded in an ENZ medium of $\epsilon_1 = 0.001\epsilon_0$. The distance between the centers of

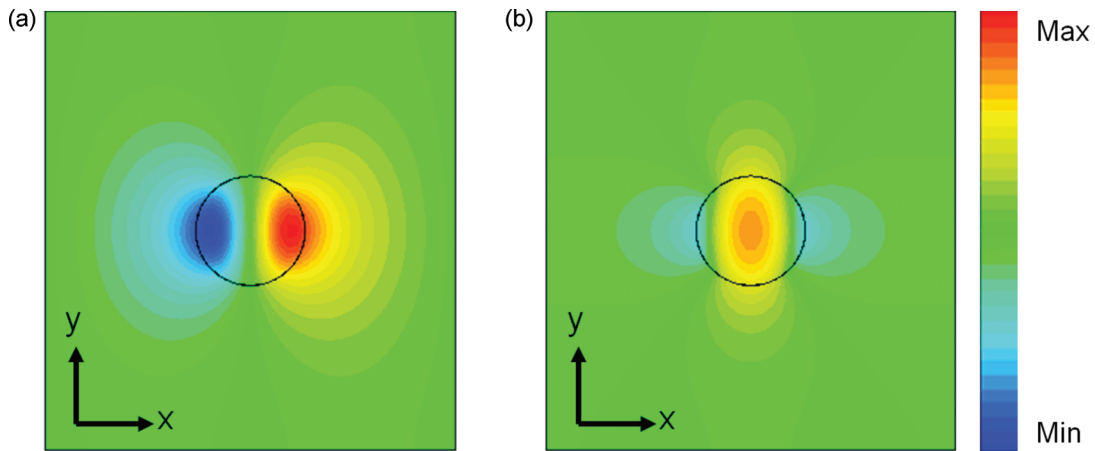


FIG. 3. (Color online) Electric E_z (a) and magnetic H_y (b) field distribution for the first resonant mode associated with the first zero of $J_0(k_2R)$ (at frequency 4.54 THz) of a single cylinder of radius $R = 4 \mu\text{m}$, the permittivity of which is $\epsilon_2 = 40\epsilon_0$ embedded in an ENZ matrix with $\epsilon_1 = 0.001\epsilon_0$, for a plane TE wave incident on the cylinder according to Microwave Studio.

the cylinders is $a_0 = 12 \mu\text{m}$. Notice the strong confinement along the chain of cylinders even if the chain is bent [Fig. 4(b)]. (This confinement provides a further justification for the omission of the couplings along the y direction.)

The dispersion relation of such a “waveguide” of cylinders has also been calculated around the frequency 4.55 THz and is shown in Fig. 5. It is evident from Fig. 5 that the guided mode is slow (its phase velocity is smaller than the free-space velocity c).

We stress again that the proposed waveguide made of a chain of cylinders in an ENZ matrix can also be used as a corner structure. For example, the E_z field distribution shown in Fig. 4(b) corresponds to a change of propagation direction by 45 deg. This is accompanied by a weak backscattering, as shown in Fig. 4(b), where part of the power is reflected at the turn and interferes with the incoming field leading to a weaker total field as the corner is approached. Nevertheless, such a system is still efficient and can be used to change the

directions of the transported energy over distances of several wavelengths.

Observing the field profile shown in Fig. 4, one can see that in contrast to the well-known similar plasmonic waveguides^{36–38} consisting of linear chains of plasmonic particles, the field of the waveguide under consideration is concentrated between the inclusions and not on the lateral sides of the waveguide. Thus, the subwavelength confinement in a single row along propagation direction is expected to be maintained even in a system of parallel rows, forming a photonic-crystal-like structure. Such a system, for subwavelength size cylinders, is expected to behave as an anisotropic lens with subwavelength resolution. To verify that, we considered such a system and we simulated (using Microwave Studio) the distribution of the electric field E_z behind a PEC (perfect electric conductor) screen with a narrow slit of width $4 \mu\text{m}$. A TE plane wave of frequency 4.55 THz is incident on the screen from the left as shown in Fig. 6(a). The frequency

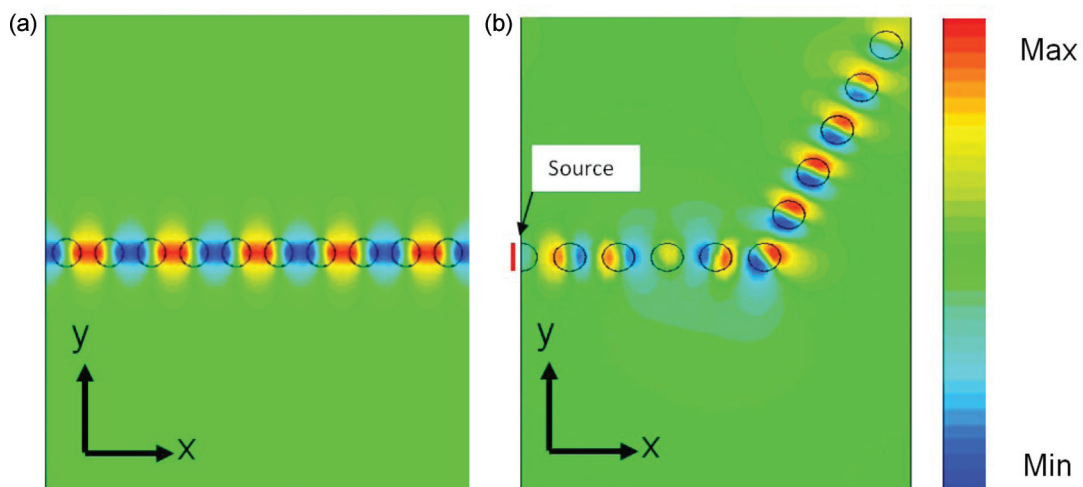


FIG. 4. (Color online) Electric E_z field distribution at the frequency 4.55 THz for: (a) a waveguide based on cylinders of radius $R = 4 \mu\text{m}$, distance $a_0 = 12 \mu\text{m}$, and permittivity $\epsilon_2 = 40\epsilon_0$, embedded in an ENZ matrix of permittivity $\epsilon_1 = 0.001\epsilon_0$; (b) a corner 45° angle structure based on the waveguide shown in (a). The field distribution has been obtained using the Microwave Studio.

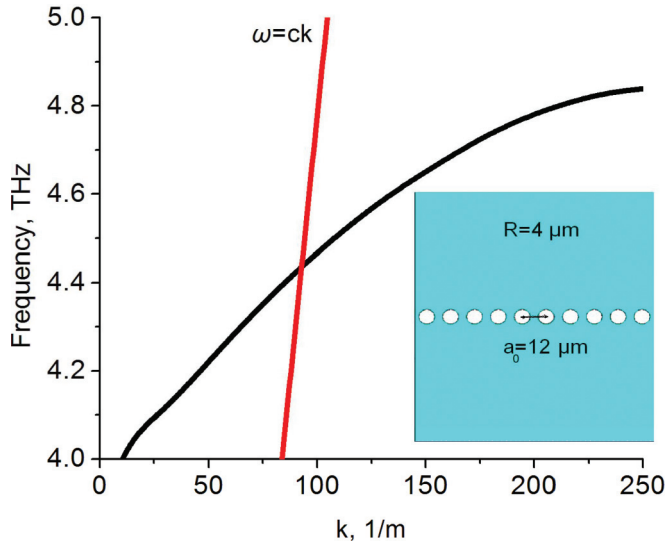


FIG. 5. (Color online) Dispersion characteristics of a waveguide based on cylinders of radius $R = 4 \mu\text{m}$ and permittivity $\epsilon_2 = 40\epsilon_0$, embedded in an ENZ matrix of permittivity $\epsilon_1 = 0.001\epsilon_0$; the distance between the cylinders is $a_0 = 12 \mu\text{m}$. The black curve shows the mode of this waveguide and the red curve the *light line* of $\omega = ck$. The inset shows a schematic of the waveguide.

of 4.55 THz corresponds to total transmission $|\bar{t}|$ ($|\bar{t}| \approx 1$) for a single cylinder in accordance with Fig. 2, as well as for the system of many cylinders [Fig. 6(b)]. Obviously the resonance of a single cylinder is broadened to a narrow band for the system of many cylinders, which proves that the origin of the total transmission and subwavelength lensing effect is a Mie resonance of a single cylinder. Figure 6(b) shows this broadening which is fully equivalent to the creation of a narrow band around an atomic orbital in the well-known tight binding (TB) model in solid state physics. As shown in Fig. 6(a), the incident wave is diffracted on the slit and excites Mie-resonance modes from the first to the next cylinder along the x direction, transferring thus the subwavelength slit image.

IV. ENHANCED TRANSMISSION THROUGH A POLARITONIC SYSTEM IN ENZ REGIME

Finally, we discuss how we can apply this theory in realistic materials with ENZ response in the THz regime. Such materials are polaritonic materials. The particular system that we will examine is a system LiF cylinders (of μm radius) embedded in KCl matrix, forming a hexagonal lattice. As it was recently shown,³⁹ such a system can be realized quite easily using a self-organization approach known as eutectics directional solidification.⁴⁰ Each of the components of our system (the LiF cylinders and the KCl host) is a polaritonic material exhibiting an electrical permittivity response of Lorenz type:^{26,27}

$$\epsilon = \epsilon_\infty \frac{\omega^2 - \omega_L^2 + i\omega\gamma}{\omega^2 - \omega_T^2 + i\omega\gamma'} \quad (11)$$

In Eq. (11) ω_T is the angular frequency of the transverse optical phonons in the polaritonic material, ω_L is the angular frequency of longitudinal optical phonons, γ is the damping factor, and ϵ_∞ is the limiting value of the permittivity for high frequencies relative to ω_L . Notice that Eq. (11) allows an ENZ response for frequencies $\omega \approx \omega_L$.

In our LiF rods in the KCl system the rod radius is $R = 1 \mu\text{m}$ and the nearest neighbor separation (from center to center) is $4 \mu\text{m}$. The KCl is determined by material parameters³⁹ $\epsilon_\infty = 2.045$, $f_T = \omega_T/2\pi = 4.21 \text{ THz}$, $f_L = \omega_L/2\pi = 6.196 \text{ THz}$, and $\gamma' = \gamma/2\pi = 0.156 \text{ THz}$, showing an ENZ response around 6 THz, while for the LiF $\epsilon_\infty = 2.0272$, $f_T = \omega_T/2\pi = 9.22 \text{ THz}$, $f_L = \omega_L/2\pi = 19.106 \text{ THz}$, and $\gamma' = \gamma/2\pi = 0.527 \text{ THz}$, giving positive values for the LiF permittivity ϵ_{LiF} at the frequency $f(= \omega/2\pi)$ range $\sim 4\text{--}8 \text{ THz}$, i.e., dielectric-like response.

The transmission coefficient for a TE polarized incident wave (electric field parallel to the cylinder axis) through a system of LiF cylinders embedded in KCl is depicted in Fig 7.

The frequency of 6 THz corresponds to the plasma frequency of KCl, i.e., $Re(\epsilon_{\text{KCl}}) \approx 0$, and $Re(\epsilon_{\text{LiF}}) = 12$. As is shown in Fig. 7, there is a quite a high transmission peak around

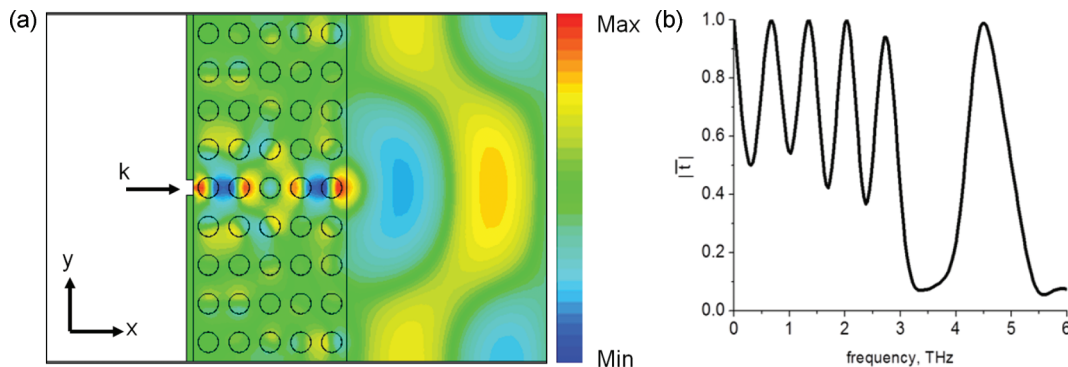


FIG. 6. (Color online) (a) The E_z field distribution for a metamaterial “lens” composed of five layers (along propagation direction) of subwavelength cylindrical inclusions of radius $R = 4 \mu\text{m}$, and permittivity $\epsilon_2 = 40\epsilon_0$, embedded in an ENZ matrix with $\epsilon_1 = 0.001\epsilon_0$. The distances between the cylinders are 12 and 15 μm , along x and y axes, respectively. The incident wave has frequency 4.55 THz. (b) Transmission coefficient $|\bar{t}|$ through the system depicted in (a); $|\bar{t}|$ has been calculated through Microwave Studio. Note that the peaks below 3 THz correspond to Fabry-Perot resonances, occurring when the system length (along the x direction) equals an integer multiple of the effective half-wavelength.

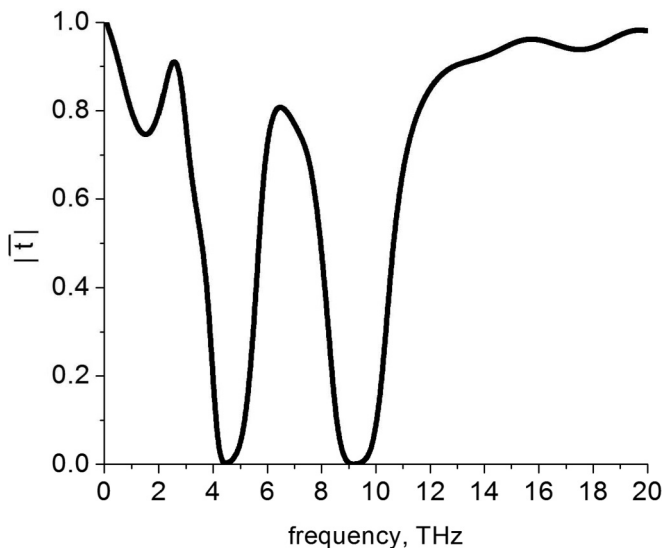


FIG. 7. Transmission coefficient $|t|$ as a function of frequency for a hexagonal lattice of LiF cylinders with radius $R = 1 \mu\text{m}$ and separation (from center to center) $4 \mu\text{m}$, embedded in a KCl matrix. The material parameters for KCl (see text) show an ENZ response around 6 THz (at which a peak in the transmission appears), while for the LiF the permittivity is positive in the frequency range 4–8 THz.

that frequency despite the substantial material losses in LiF and KCl. Note also the quite broadband character of the peak. Of course, in this case, we cannot achieve total transmission of EM waves through the structure because the materials exhibit losses; we see that the losses, unless they are very large, do not quite eliminate the substantial increase of the transmission coefficient due to Mie resonances in the cylindrical inclusions and the transfer of these quasi bound states along the linear periodic arrangement of identical scatterers.

Finally, one should pay attention to the fact that in the case of an ENZ matrix it is not necessary to use dielectrics with large values of permittivity to achieve deep subwavelength resonances and thus metamaterial phenomena associated with high-permittivity materials, such as artificial magnetism and negative refractive index. Even moderate permittivity inclusions can lead to such phenomena since the relevant parameter is the ratio $\varepsilon_2/\varepsilon_1$ which must be much larger than one. This is extremely beneficial in metamaterial-based applications, as high permittivity materials are usually associated with high material losses. Moreover, high permittivity materials are more and more difficult to find as one goes to higher frequencies, approaching the optical regime.

V. CONCLUSIONS

In conclusion, we have studied and analyzed the transmission through systems of subwavelength dielectric cylinders embedded in an ENZ host. It is shown that due to Mie resonances associated with a p_x -like distribution of the electric field in the dielectric cylinders the transmission is strongly enhanced. Subwavelength waveguides and lenses

have been proposed based on this enhanced transmission and the associated subwavelength confinement of the wave in the direction perpendicular to that of the waveguide. Finally, we showed that these interesting properties in the THz regime can be realized in a self-organized polaritonic system of LiF cylinders embedded in KCl host.

ACKNOWLEDGMENTS

Authors acknowledge financial support by Greek GSRT through the project ERC-02 EXEL, and by the EU project ENSEMBLE (Grant Agreement No. 213669), and the COST Action MP0803. Work at Ames Laboratory was partially supported by the US Department of Energy (Basic Energy Sciences, Division of Materials Sciences and Engineering), Contract No. DE-AC02-07CH11358, and by the US Office of Naval Research (Award No. N00014-10-1-0925). Work at National Research University “Moscow Power Engineering Institute” was supported by RFBR (Grant Agreements No. 13-02-00732 and No. 13-08-01278) and Russian Federal Program “Scientific and scientific-pedagogical Staffs of Innovative Russia” for 2009–2013 (Agreement No. 14.B37.21.1211).

APPENDIX

As was mentioned in the text, to take into account in our analytic formulas the periodicity of the system of Fig. 1 along the y direction, one should also take into account the fields incident on the $n = 0$ cylinder along the y direction due to the presence of all the other cylinders. This field will come basically from the omnidirectional component of the scattered field from the other cylinders along y (see Sec. II) and can be approximately taken into account as follows: The cylinder located at the n th unit cell in the y direction will emit an omnidirectional wave which at reaching the cylinder located at $n = 0$ will have an amplitude $E/(-i\omega\mu) = \Gamma_0 X_0(nk_1 d)$ (omitting any scattering in its travel from the $n \neq 0$ to the $n = 0$ cylinder) and it will induce an additional omnidirectional scattered wave of strength equal to $\Gamma_0 X_0(nk_1 d) \bar{A}_{0s}$, according to (8b). Thus, to first order, all the cylinders in the y direction will produce at the $n = 0$ cylinder an additional scattered wave of strength $\Gamma_0 \bar{X}_0 \bar{A}_{0s}$, where $\bar{X}_0 = \sum_{n=1}^{+\infty} X_0(nk_1 d) + \sum_{n=-1}^{-\infty} X_0(nk_1 d) = 2 \sum_{n=1}^{+\infty} X_0(nk_1 d)$. This, in turn, will renormalize A_{0s} to $A_{0s} + \Gamma_0 \bar{X}_0 \bar{A}_{0s}$ and Γ_0 to $\bar{\Gamma}_0 = (A_{0s} + \bar{\Gamma}_0 \bar{X}_0 \bar{A}_{0s}) / (1 + A_{0s} \bar{F}_0 + \bar{\Gamma}_0 \bar{X}_0 \bar{A}_{0s} \bar{F}_0)$, where $\bar{F}_0 = \bar{X}_0(s) - s \bar{X}'_0(s) / i\omega$. In the present case $A_{0s} = \bar{A}_{0s}$ since $\eta = 1$ [see Eq. (9)]. The summation $\sum_{n=1}^{+\infty} X_0(nk_1 d)$ can be performed in terms of the integral $\int_{k_1 d}^{+\infty} X_0(x) dx$ by using the Euler-Maclaurin summation formula.⁴¹ We should mention that the renormalization described above and due to the couplings among cylinders in the y direction as a result of the periodicity along the y direction, is correct to the first order only since multiple scattering effects involving both the plane surfaces at $x = 0$ and $x = a$ and the cylinders located at $n \neq 0$ were omitted. For large d , $d \geq 100 \mu\text{m}$, these y -direction couplings are negligible, as the numerical calculations have shown.

*basharin@iesl.forth.gr

- ¹V. G. Veselago, *Sov. Phys. Usp.* **10**, 509 (1968).
- ²J. B. Pendry, *Phys. Rev. Lett.* **85**, 3966 (2000).
- ³N. I. Zheludev, *Science* **328**, 582 (2010).
- ⁴C. M. Soukoulis and M. Wegener, *Science* **330**, 1633 (2010).
- ⁵A. Boltasseva and H. A. Atwater, *Science* **331**, 290 (2011).
- ⁶C. M. Soukoulis and M. Wegener, *Nat. Photon.* **5**, 523 (2011).
- ⁷Y. Liu and X. Zhang, *Chem. Soc. Rev.* **40**, 2494 (2011).
- ⁸P. Tassin, T. Koschny, M. Kafesaki, and C. M. Soukoulis, *Nat. Photon.* **6**, 259 (2012).
- ⁹C. Pecharroman, F. Esteban-Bategon, J. F. Bartolomé, S. López-Esteban, and J. S. Moya., *Adv. Mater.* **13**, 1541 (2001).
- ¹⁰M. Silveirinha and N. Engheta, *Phys. Rev. B* **76**, 245109 (2007).
- ¹¹M. Silveirinha and N. Engheta, *Phys. Rev. Lett.* **97**, 157403 (2006).
- ¹²M. Silveirinha and N. Engheta, *Phys. Rev. E* **78**, 016604 (2008).
- ¹³B. Edwards, A. Alù, M. E. Young, M. Silveirinha, and N. Engheta, *Phys. Rev. Lett.* **100**, 033903 (2008).
- ¹⁴R. Liu, Q. Cheng, T. Hand, J. J. Mock, T. J. Cui, S. A. Cummer, and D. R. Smith, *Phys. Rev. Lett.* **100**, 023903 (2008).
- ¹⁵R.W. Ziolkowski, *Phys. Rev. E* **70**, 046608 (2004).
- ¹⁶J. Hao, W. Yan, and M. Qiu, *Appl. Phys. Lett.* **96**, 101109 (2010).
- ¹⁷V. C. Nguyen, L. Chen, and K. Halterman, *Phys. Rev. Lett.* **105**, 233908 (2010).
- ¹⁸Y. Xu and H. Chen, *Appl. Phys. Lett.* **98**, 113501 (2011).
- ¹⁹S. Enoch, G. Tayeb, P. Sabouroux, N. Guérin, and P. Vincent, *Phys. Rev. Lett.* **89**, 213902 (2002).
- ²⁰A. Alù, M. G. Silveirinha, A. Salandrino, and N. Engheta, *Phys. Rev. B* **75**, 155410 (2007).
- ²¹R. J. Pollard, A. Murphy, W. R. Hendren, P. R. Evans, R. Atkinson, G. A. Wurtz, A. V. Zayats, and V. A. Podolskiy, *Phys. Rev. Lett.* **102**, 127405 (2009).
- ²²X. Huang, *Nat. Mater.* **10**, 582 (2011).
- ²³J. Luo, *Appl. Phys. Lett.* **100**, 221903 (2012).
- ²⁴S. Campione, M. Albani, and F. Capolino, *Opt. Mater. Express* **1**, 1077 (2011).
- ²⁵Y. Jin and S. He, *Opt. Express* **18**, 16587 (2010).
- ²⁶Neil W. Ashcroft and N. David Mermin, *Solid State Physic* (Holt, Rinehart and Winston, New York, 1976).
- ²⁷E. D. Palik, *Handbook of Optical Constants of Solids* (Academic, Orlando, 1985).
- ²⁸L. D. Landau, E. M. Lifshitz, and L. P. Pitaevskii, *Electrodynamics of Continuous Media*, 2nd ed. (Pergamon, Oxford, 1984).
- ²⁹H. C. Van der Hulst, *Light Scattering by Small Particles* (John Wiley and Sons, New York, 1957).
- ³⁰S. O'Brien and J. B. Pendry, *J. Phys.: Condens. Matter* **14**, 4035 (2002).
- ³¹L. Peng, L. Ran, H. Chen, H. Zhang, J. A. Kong, and T. M. Grzegorzcyk, *Phys. Rev. Lett.* **98**, 157403 (2007).
- ³²J. A. Schuller, R. Zia, T. Taubner, and M. L. Brongersma, *Phys. Rev. Lett.* **99**, 107401 (2007).
- ³³M. S. Wheeler, J. S. Aitchison, and M. Mojahedi, *Phys. Rev. B* **72**, 193103 (2005).
- ³⁴L. Jylhä, I. Kolmakov, S. Maslovski, and S. Tretyakov, *J. Appl. Phys.* **99**, 043102 (2006).
- ³⁵K. C. Huang, M. L. Povinelli, and J. D. Joannopoulos, *Appl. Phys. Lett.* **85**, 543 (2004).
- ³⁶S. A. Maier, M. L. Brongersma, and H. A. Atwater, *Appl. Phys. Lett.* **78**, 16 (2001).
- ³⁷S. A. Maier, P. G. Kik, and H. A. Atwater, *Phys. Rev. B* **67**, 205402 (2003).
- ³⁸A. Alù, P. A. Belov, and N. Engheta, *Phys. Rev. B* **80**, 113101 (2009).
- ³⁹A. Reyes-Coronado, M. F. Acosta, R. I. Merino, V. M. Orera, G. Kenanakis, N. Katsarakis, M. Kafesaki, Ch. Mavidis, J. García de Abajo, E. N. Economou, and C. M. Soukoulis, *Opt. Express* **20**, 14663 (2012).
- ⁴⁰J. Llorca and V. M. Orera, *Prog. Mat. Sci.* **51**, 711 (2006).
- ⁴¹M. Abramowitz and I. A. Stegun (eds.), *Handbook of Mathematical Functions* (Dover, NY, 1972), p. 16.